



VIRTUAL PROTOTYPING OF ADHESIVELY RESTORED, ENDODONTICALLY TREATED MOLARS

Pascal Magne, DMD, PhD^a

University of Southern California, Herman Ostrow School of Dentistry, Los Angeles, Calif

Statement of problem. Teeth and dental restorations are difficult to model because of their complex anatomical shape and layered structure.

Purpose. The purpose of this investigation was to describe the use of an efficient virtual prototyping method for the comparison of bonded porcelain and composite resin onlays to restore endodontically treated molars.

Material and methods. An intact mandibular molar was digitized with a micro-CT scanner. Surface contours of enamel and dentin were fitted following tooth segmentation based on pixel density using an interactive medical image processing software (Mimics). Standard triangle language files of enamel and dentin surfaces were then exported to a design and meshing software (3-matic). The root filling, base material, and a 3.0-mm-thick onlay were created by merging primitive shapes. Surface splitting, removal of unwanted surfaces, and remeshing allowed generation of an assembly with optimized interfacial mesh congruence and T-junctions. Solid 3-dimensional (3-D) models obtained in a finite element software (Marc/Mentat) were subjected to nonlinear contact analysis to simulate occlusal loading at 200 N and 700 N. Maximum principal stress values were used to calculate the risk of fracture and for validation with existing experimental data.

Results. There were similar stress distributions at 200 N (maximum peak values of 24 to 26 MPa) for both restorative materials, but marked differences at 700 N, with the porcelain onlay showing occlusal stress peaks more than 30% higher than composite resin. High stress concentrations were found at 700 N at the root level of the porcelain-restored tooth (95 MPa). For the composite resin onlay, secondary peaks of stress at the 700-N load were found above the cemento-enamel junction (47 MPa) with only minor effects at the root. The risk of fracture was increased for porcelain onlays, which correlated with the existing validation data and the decreased risk of fracture below the cemento-enamel junction (CEJ) observed for composite resin onlays.

Conclusions. The virtual prototyping method can generate detailed and valid 3-D finite element models of a restored, endodontically treated molar. The decreased risk of fracture and more favorable stress distribution of adhesive composite resin onlays compared to porcelain onlays were confirmed. This method is efficient and may be used for other medical and dental applications. (J Prosthet Dent 2010;103:343-351)

CLINICAL IMPLICATIONS

Advances in virtual prototyping not only facilitate optimization and understanding of biomedical devices but will allow creation of patient-specific numeric models from any body part using either MRI, micro-CT, or cone beam CT data. For the restorative dentist, the ability to predict tooth/restoration failure is an example of the diagnostic value of virtual prototyping.

This study was supported in part by MSC Software Corp (Marc/Mentat products) and Materialise (Mimics and 3-matic products).

^aAssociate Professor of Dentistry, Oral Health Center, and The Don and Sybil Harrington Foundation Professor of Esthetic Dentistry.

MAGNE



Due to the costs and risks involved in *in vivo* studies, numeric models and *in vitro* simulation approaches are gaining interest among scientists¹ and manufacturers of biomedical devices. Study design analysis is first accomplished on the computer and/or in the simulated oral environment. When the best design or material has been refined, the actual experiment may be conducted. The modeling and simulation step saves time and costs and reduces the risk of conducting the study or clinical trial *in vivo*.

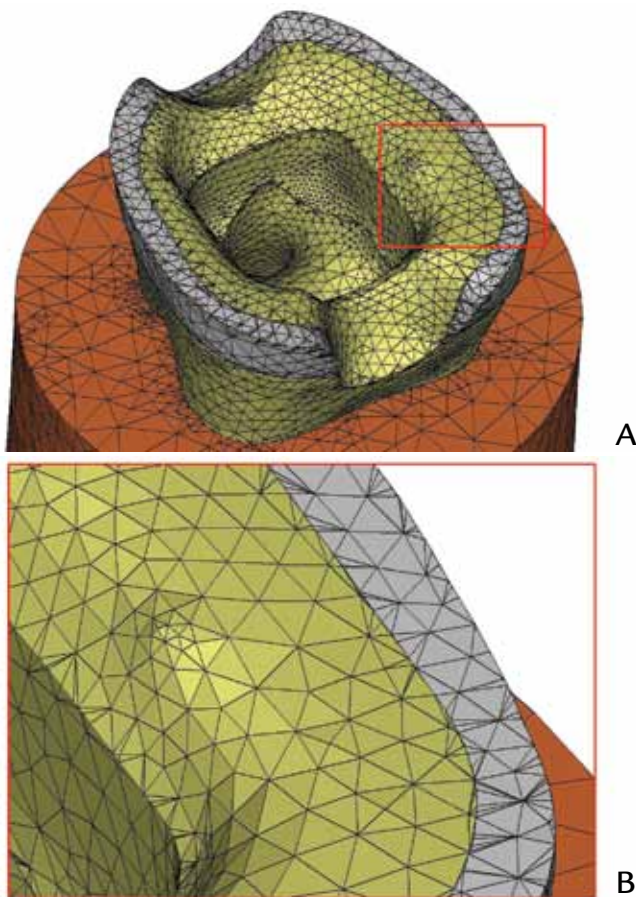
The biomedical industry has long benefited from virtual prototyping (numeric simulation) using finite element (FE) analysis to improve products, allowing enhancement of development, design, engineering, testing, certification, and production. The use of FE analysis in dental research has been significantly refined during the last decade.²⁻⁹ Using the traditional biophysical knowledge database in a rational validation process,¹⁰ hybrid experimental-numeric approaches (combining a real physical experiment and a virtual numeric model) represent the most comprehensive *in vitro* investigation methods in restorative dentistry.^{8,9} Significant advantages include the reduced time and cost to bring a new idea from concept to clinical application and the increased confidence in the final concept/project.

Unlike medical devices, teeth and bones cannot be assimilated to a simplified geometric representation but have anatomical shapes and a layered structure. As a result, geometry acquisition has often appeared to be the most time-consuming step for the modeler. The limits of computational power have also been a significant factor in keeping numeric models as simple as possible by making them grossly 3-dimensional (3-D), with a substantial compromise in geometry,¹¹ or by converting problems into axisymmetric and 2-dimensional (2-D) situations.¹²⁻¹⁴ For specific problems that are 3-D by nature, such as the simulation of the endodontically treated tooth, 2-D models are not

applicable, unless some “artificial compensation” tools are applied, such as the inclusion of side plates.¹² Because of technological advances, the last decade has been marked by the transition from gross 3-D and simplified 2-D models to sophisticated 3-D techniques. Computerized tomography (CT) scan-based FE models⁵ have made it possible to generate refined geometries, minimize errors, simplify the process, and reduce the risk of faulty predictions. The use of microscale CT scanners has been proposed for geometry acquisition for small objects such as teeth, dental implants, and dental restorations.¹⁵ A considerable amount of work was initially required to obtain congruent parts (sharing the exact same geometry at their interface) and smooth relationships between the different 3-D objects (enamel, dentin, restoration). Innovative virtual prototyping

softwares were developed to resolve these problems. Using standard triangle language (STL) and Boolean operations (addition, intersection, or subtraction of volumes) to simulate tooth substance removal and restorative processes, recent advances have not only further simplified geometry acquisition but also geometry modification during the fabrication of valid FE models of dental restorations.¹⁶⁻¹⁹

Constant refinements of the technique are occurring. Among other challenges, thin shell intersections, such as those in enamel, constitute a particular difficulty in the meshing process because intersecting surfaces generated by Boolean operations may produce faulty meshes at some specific locations. Intersection zones, also called T-mesh areas, present a distinct challenge and may result in poor quality meshes (skewed elements) and a partial lack of congruency (Fig. 1).



1 A, Example of faulty mesh generated by Boolean operation to simulate total cuspal coverage on endodontically treated tooth. B, Detailed view (red rectangle in A): note skewed triangles, irregular mesh, and lack of congruency between enamel (gray) and dentin (yellow) at T-junction (dentino-enamel junction, or DEJ).

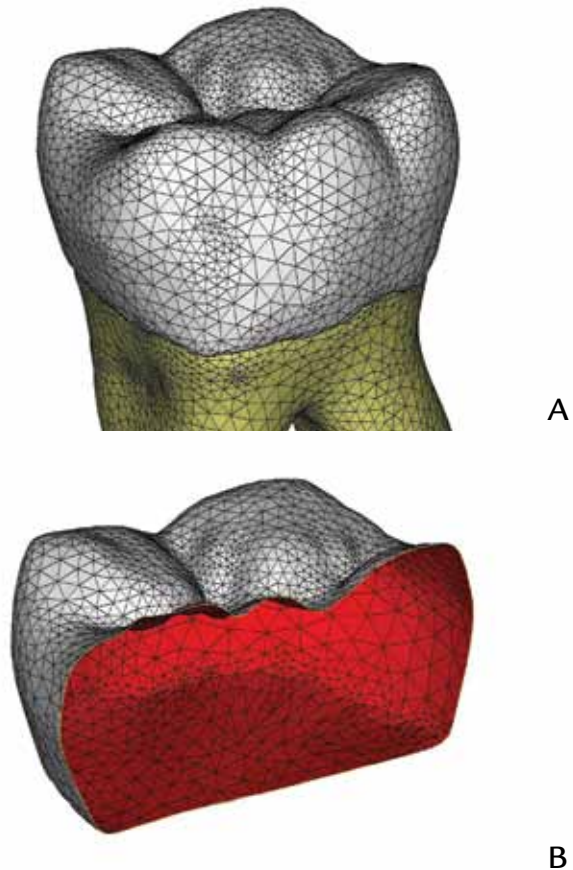
While those “errors” are not critical for simple models with bulk structures, they may be problematic in rendering more complex structures with multiple thin layers and shells.

The purpose of this study is, therefore, to propose an additional refinement in the development of a fully congruent interfacial mesh between different objects during the fabrication of FE models of tooth restorations. The virtual prototyping method is based on STL combined with surface-driven automatic meshing using an advanced STL design and meshing software. A complex model of a restored, endodontically treated molar is built in multiple surfaces using surface splitting and the creation of self-intersection curves with CAD objects instead of Boolean operations.

MATERIAL AND METHODS

A 3-D FE model of a human mandibular molar was generated in 4 steps. First, a high-resolution micro-CT scanner (SkyScan 1072 micro-CT; SkyScan, Aartselaar, Belgium) was used to scan the tooth at a voxel dimension of 13.65 μm (slices obtained during previously published study¹⁶). Two frames were taken per angle, and there were 208 angles. Exposure time was 7.2 s/frame. One slice out of every 14 slices was used for the modeling (81 slices out of 1128 slices).

Second, an interactive medical image processing software (Mimics 9.0; Materialise, Leuven, Belgium) allowed identification of the different hard tissues visible on the scans. Mimics features extended visualization and segmentation functions based on image density thresholding. Each 3-D object is created by growing a threshold region on the entire stack of scans. Each resulting mask (enamel, dentin) is then converted into a 3-D file (STL, bilinear, and interplane interpolation algorithm) using the Mimics STL+ module. Because of the aspect ratio and connectivity of the triangles in the native STLs, these files are inappropriate for use in FE analysis (FEA). Reducing the number of triangles and simultaneously improving the quality



2 A, Enamel and dentin STL files as generated by Remesh module in Mimics. B, Enamel shell following removal of DEJ and closing of resulting hole with fix wizard in 3-matic.

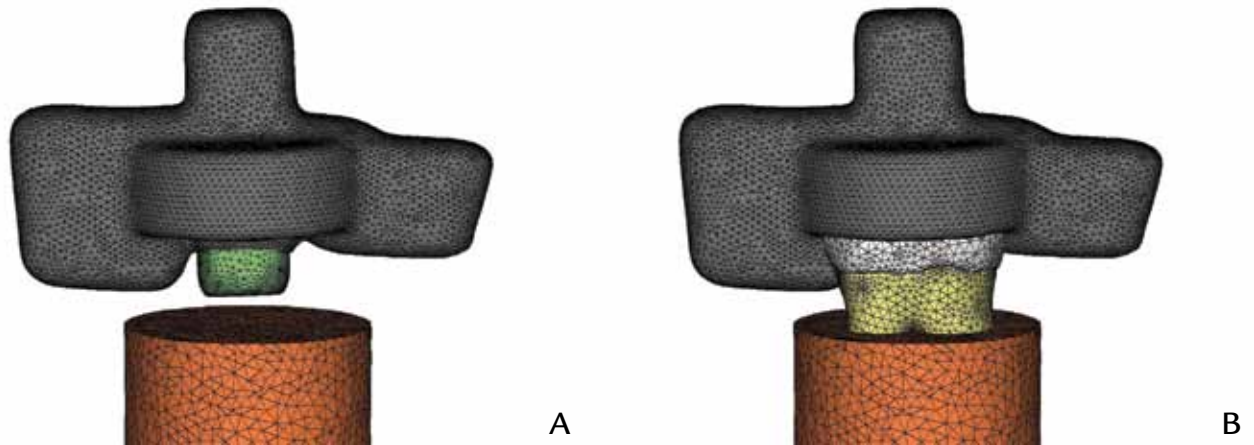
of the triangles while maintaining the geometry is automatically achieved with the Remesh component included with Mimics (Fig. 2).

Third, an advanced STL design and meshing software (3-matic 4.2; Materialise) was used: (1) to generate additional intersection parts simulating the endodontic access and onlay preparation, and (2) to establish perfect congruence of the interfacial mesh between the different objects (enamel, dentin, endodontic base material, restorative material, bone). To begin with, the dentino-enamel junction (DEJ) portion of the enamel was removed. The resulting hole was closed using the fix wizard built into 3-matic (Fig. 2, B).

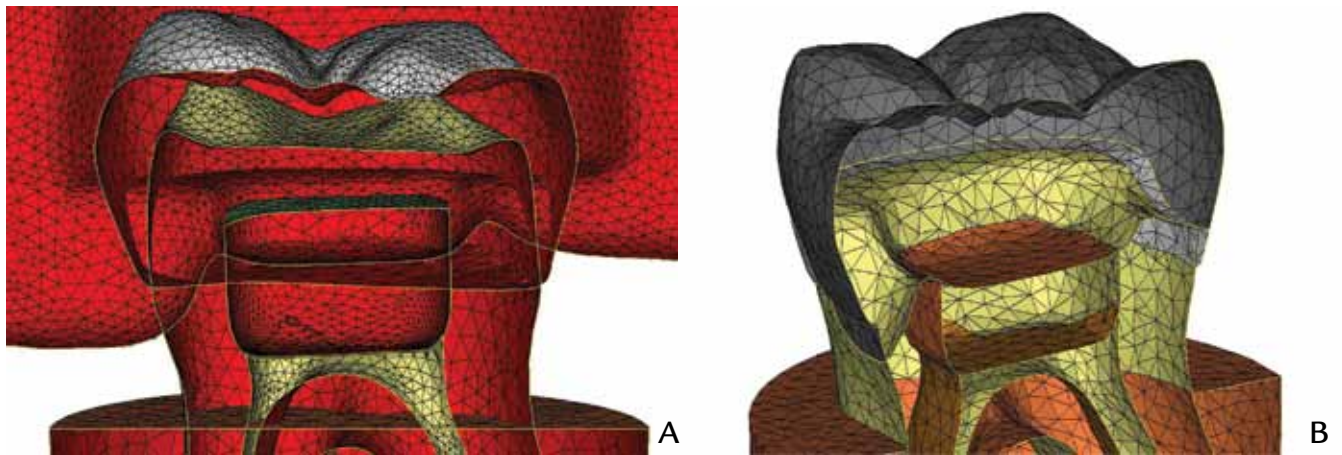
Primitive shapes (mainly rounded inserts and cylinders) were then created, merged, and smoothed to create parts corresponding to the main intersecting volumes (Fig. 3), as well as a cylindrical fixation base (embed-

ding the root within 3 mm of the CEJ).

The following sequence was then applied (Fig. 4), beginning with the merging of all 5 parts (2 intersecting CAD objects, enamel, dentin, and fixation base) into a single STL file called the *assembly*. Self-intersecting curves were then created and used to split all triangles at the intersections within the assembly. Using a section view to look inside the assembly, all unwanted surfaces were deleted. The definitive assembly was then remeshed using the 3-matic Remesh component. Self-intersecting curves were maintained and the tolerance variation from the original data was specified (quality of triangles does not mean tolerance variation from the original data). As in Mimics Remesh, the quality is defined as a measure of triangle height/base ratio (defined at 0.3) so that the file can be imported in the FEA software package without generating errors. Finally, the



3 A, Primitive shapes created within 3-matic to be used as subtraction/intersection volumes with enamel and dentin. B, Intersecting assembly. Gray: intersection with enamel and dentin will result in onlay restorative material. Green: intersection with dentin and pulp will result in endodontic preparation and glass-ionomer base material. Orange: cylindrical fixation base.



4 A, Cross-section view of shell assembly during the merging/splitting and removal of unwanted surfaces. B, View of definitive assembly (definitive parts) following removal of unwanted surfaces and final remeshing.

remeshed assembly was split again by indicating the proper surfaces constituting each part (onlay, glass-ionomer base, gutta-percha, enamel, dentin, and bone), separating them, and copying them as a new and definitive STL file.

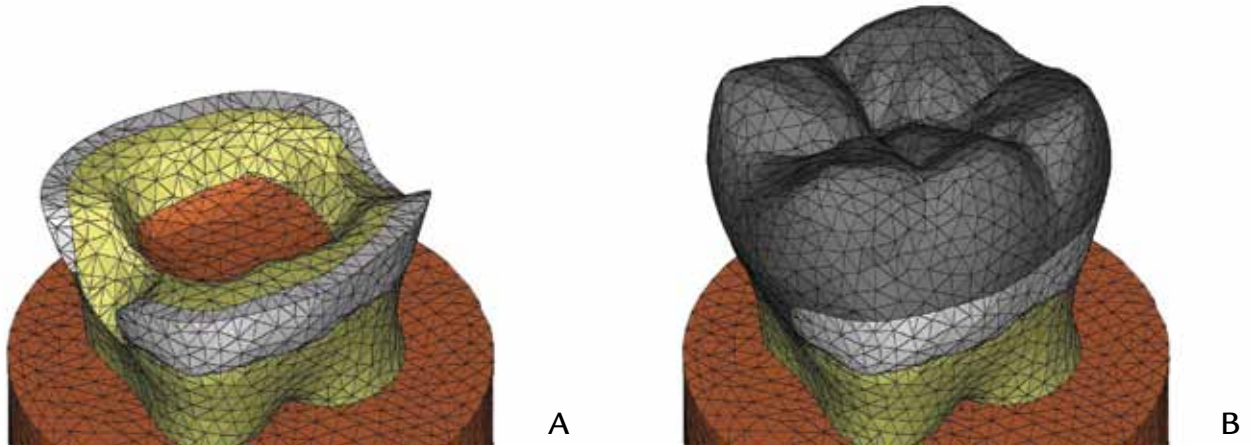
The exact design and dimensions of the onlay and glass-ionomer base reproduced existing experiments,^{20,21} which were used in the validation process for the FEA model (see Results section). The assembly consists of a prepared tooth (3.0-mm occlusal reduction, mesial and distal rounded boxes 1.5 mm below and 0.5 mm coronal to the CEJ, respectively), a root canal filled with gutta-percha, a 2.5-mm-thick glass-ionomer barrier (closing the base of the endodontic

access), and a 3.0-mm-thick onlay restoration (Figs. 4 and 5).

Fourth, the definitive STL files of all parts were then imported into an FEA software package (Marc/Mentat; MSC Software Corp, Santa Ana, Calif) for the generation of a volumetric mesh (total of 61,616 elements/12,329 nodes) and attribution of material properties according to existing data (Table I).²²⁻³² Automatic mesh generation using a tetrahedral mesher (tetrahedron elements with pyramidlike shape and 4 nodal points) is ideally achieved using the triangulated files generated in 3-matic.

The nodes at the bottom surface of the stone base were assigned fixed zero displacement in the 3 spatial di-

mensions. To simulate usage of adhesive luting cements, the tooth and restorative materials were considered to be bonded. A uniform ramp loading was applied to the mesiobuccal, mesiolingual, and distobuccal cusps (tripod contact) through a rigid body; that is, a 9.5-mm-diameter ball positioned as closely as possible to the tooth (Fig. 6). The tooth was defined as a deformable contact body. Contact between these bodies was determined automatically by the FEA simulation during the static mechanical load case (no inertia effects) with a uniform stepping procedure of 10-14 steps. A motion was applied to the rigid ball along the z-axis through a negative velocity of 0.019-0.071 mm/step, depending on the target

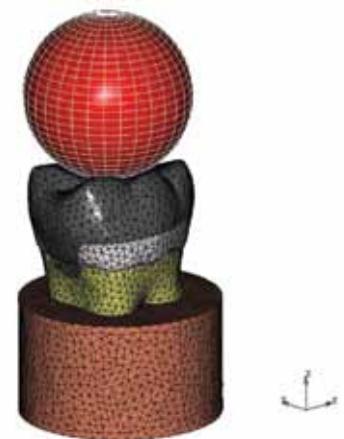


5 View of final mesh used for automatic volume mesh generation in Mentat. A, Tooth preparation with glass-ionomer base filling endodontic access cavity. B, Restored tooth with onlay.

TABLE I. Material properties

Source	Elastic Modulus (GPa)	Poisson's Ratio
Enamel	84.1 ²⁴	0.30 ²³
Dentin	18.6 ²⁸	0.31 ²⁶
Composite resin	10.0 ²⁵	0.24 ³⁰
Porcelain	78.0*	0.28 ²³
Glass-ionomer base	6.3 ³¹	0.35 ²²
Gutta-percha	0.186 ²⁷	0.49 ³²
Base (cortical bone)	14.7 ²⁹	0.30 ²⁶

*Data obtained from manufacturer of porcelain (Creation Willi Geller Intl GmbH, Meiningen, Austria)



6 View of final volumetric mesh and load sphere as seen in Mentat (preprocessing); all nodes at bottom of cylindrical fixation base were assigned fixed zero displacement in 3 spatial dimensions, and load sphere was set to move against tooth along z-axis while touching mesiobuccal, mesiolingual, and distobuccal cusps.

load. Only a single step was required to reach contact in both cusps. The motion continued for the remaining steps to reach a total force of 200 N or 700 N on the ball. The stress and strain distributions were solved using the MSC Marc solver (MSC Software Corp). These specific boundary conditions, load protocol, and configuration were selected because they reproduce previous experiments.^{20,21}

RESULTS

The postprocessing file was accessed through Mentat (MSC Soft-MAGNE

ware Corp). Values of maximum principal stress (primarily located at the central groove and at the distal surface of the distal root) are presented in Table II and illustrated in Figures 7 through 9. Similar stress distributions were noted at low load (200 N) with almost identical maximum peak values of 24 to 26 MPa (central groove) for both restorative materials. There were marked differences at high load, with the porcelain onlay showing stress peaks 30-50% higher than composite resin. Another major difference noted at high load was the location of secondary stress concentrations, with

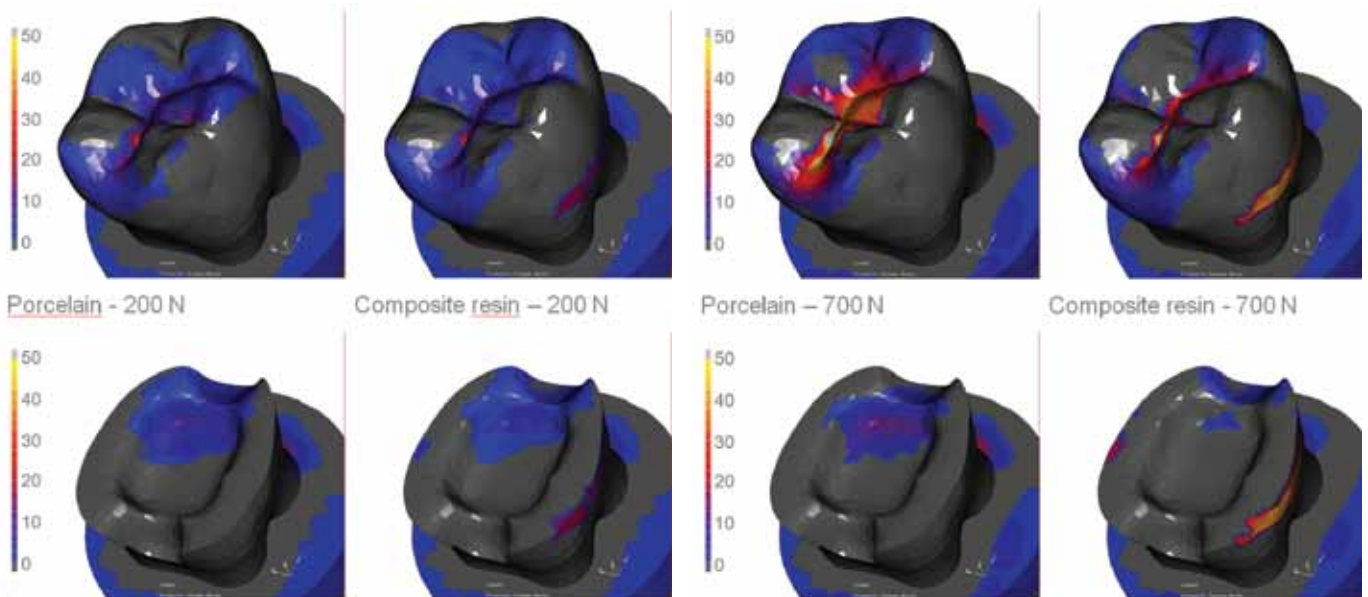
a peak value of 71 MPa at the root level for the porcelain (50% higher than composite resin at the same location). For the composite resin onlay, the secondary peak of stress at the 700-N load was found at the buccal surface instead (47 MPa) with only minor effects at the root level. This secondary peak was visible at 200 N.

The FEA model in the present study is a reproduction of restorative conditions simulated in 2 consecutive experiments, in which porcelain restorations failed first, at loads between 600 N and 800 N.^{20,21} Figure 10 shows the difference in survival



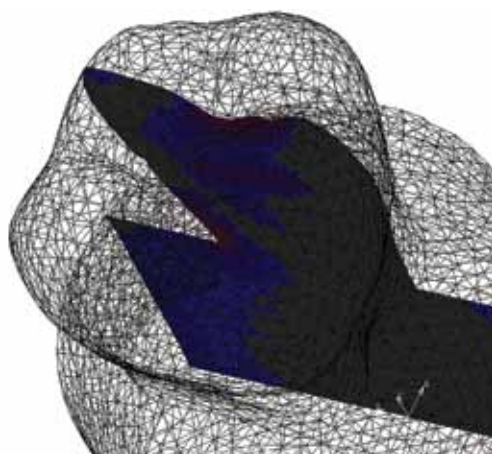
TABLE II. Areas of maximum principal stress in MPa

Restorative Material	200-N Occlusal Load		700-N Occlusal Load	
	Maximum Principal Stress at Central Groove	Secondary Maximum Principal Stress	Maximum Principal Stress at Central Groove	Secondary Maximum Principal Stress
Composite resin	24.2	18.7 (buccal surface) 24.2 (root)	60.2	47.0 (buccal surface) 33.9 (root)
Porcelain	26.4	26.4 (root)	95.4	71.16 (root)

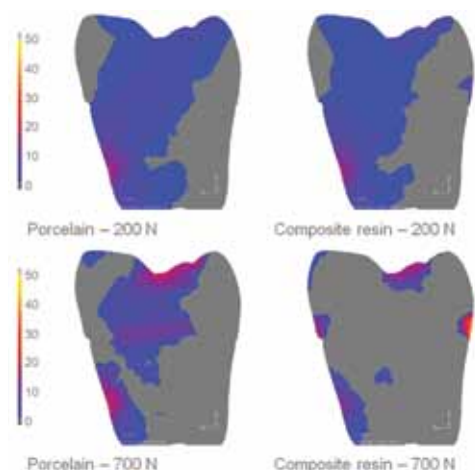


7 Maximum principal stress (MPa) as seen in Mentat with 200-N occlusal loading. Note similar stress distribution for both materials (restoration was set as “invisible” in lower images).

8 Maximum principal stress (MPa) as seen in Mentat with 700-N occlusal loading. Note different stress distribution with higher tensile stresses at occlusal surface (especially central groove) for porcelain restoration and higher stresses at buccal margin for composite resin restoration.

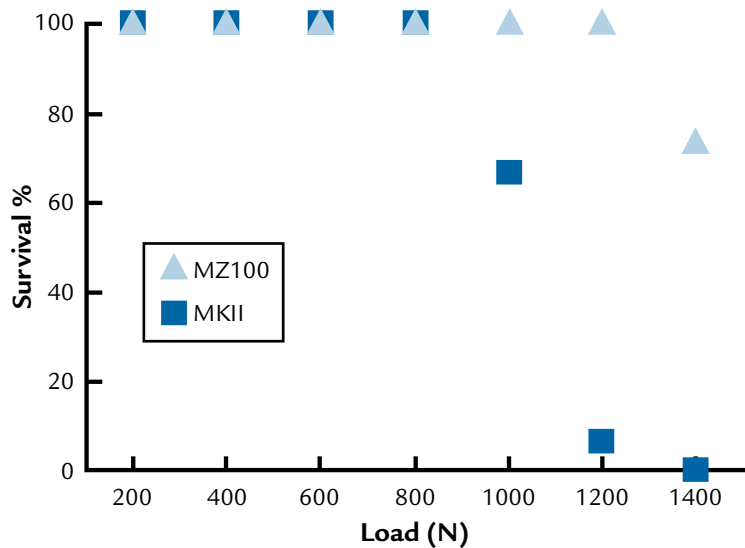


A



B

9 A, Maximum principal stress (MPa) as seen in Mentat when using section views across distal root. B, Note similar stress distribution for both materials with 200-N occlusal loading compared to 700 N.



10 Fatigue survival scatter plot²⁰ of composite resin (MZ100; 3M ESPE, St. Paul, Minn) versus porcelain (VITA MKII; Vident, Brea, Calif) onlays in endodontically treated molars with same restorative design as in present FEA study. (Figure adapted from previously published figure.²⁰ Reproduced with permission from Quintessence Publishing Co, Inc.)

rates for both restorative materials when subjected to cyclic loading. While none of the porcelain onlays survived the test (average failure load of 1147 N), composite resin onlays did not fail in 70% of the specimens. Because all fractures appear to start at the occlusal surface, the level of fracture risk in the corresponding FEA model can be evaluated quantitatively by the following equation:

Fracture risk = maximum principal stress (occlusal surface)/ultimate tensile strength (UTS).

Above a value of 1, the risk of fracture increases with the calculated value. For porcelain (UTS of 25 MPa), the ratio goes from 0.97 at 200 N (24.2 MPa/25 MPa) to 3.8 at 700 N (95.4 MPa/25 MPa). For composite resin (UTS of 40 MPa), the risk is decreased to 0.6 at 200 N (24.2 MPa/40 MPa) and 1.5 at 700 N (60.2 MPa/40 MPa). Those results are in agreement with the survival analysis in the fatigue experiment. A second indication that the model can be deemed valid is the decrease in percentage of fracture below the CEJ observed for composite resin onlays in the fatigue study,²⁰ for which the numeric model clearly

showed that secondary stresses were found above the CEJ. However the secondary stresses in the model were found more “subgingivally,” at the root level for porcelain.

DISCUSSION

In the current study, the virtual prototyping method resulted in valid, complex 3-D models with detailed tooth anatomy and a realistic computation process. The surface-based meshing not only allowed precise modeling of the challenging T-sections but also the optimization of triangle number and aspect ratio. Despite its increased complexity, the model is characterized by a reduction of 50% in the number of elements when compared to a simpler model of an MOD-restored molar in a previous, similar work.¹⁶ Cohesive relationships were simulated between the various components and were confirmed by previous studies^{20,21} in which no adhesive failures were found. The use of an optimized STL-based mesh to generate a tetrahedral volume mesh has been validated in several instances,¹⁶⁻¹⁹ and this constitutes a further indication that such models may be used for failure prediction.

The 4-step process used in the present study can be repeated and reproduced. The different parts of the model featuring different mechanical properties are identified first (segmentation process) and meshed accordingly in Mimics (Materialise). Because of the splitting of surfaces and removal of unwanted surfaces in 3-matic (Materialise), elements do not overlap the different structures but strictly follow the internal boundaries, resulting in a smooth and well controlled representation of interfaces such as the dentino-enamel junction (Fig. 5). Significant advantages, when using 3-matic, are the sophisticated visualization tools (shaded wireframe 3-D views, section views) and possibilities offered by the combination of various primitive shapes to “digitally” simulate successive restorative procedures. Measurements and rapid modifications of the different parts and generation of new STLs are enabled by the user-friendly graphic interface of 3-matic. The new parts can be instantly exported and volumetrically meshed in the FEA program.

This creates the possibility of generating instant patient-specific models with predictive values for different restorative options. It is obvious that the micro-CT technology is not yet suitable for human subjects. However, only 81 slices were necessary to generate these valid FEA models. It would seem that the rapid development of commercial dental CT-scanners, computer processing power, and interface friendliness will make this approach fast and fully automated in the near future. Intraoral scanning systems such as CEREC 3D (Sirona Dental Systems GmbH, Bensheim, Germany) are confirming this trend. These systems make extensive use of STL technology for geometry acquisition and restoration design. These data could be readily integrated into the aforementioned process.

According to the results of this simulation study, the choice of composite resin instead of porcelain seems to be indicated for onlay-type restorations of endodontically

treated teeth, especially in patients with high masticatory forces and suspected parafunctional habits such as bruxism. In the molar region of healthy young adults, maximum occlusal forces range between 597 N for women and 847 N for men and can reach over 900 N.^{33,34} The results of the present study confirm the findings of Brunton et al,³⁵ who demonstrated the greater compressive strength of composite resin onlays (1500 N) compared to ceramic onlays (990 N) in a simple load-to-failure test. In a fatigue study using low loads, Attia et al³⁶ were not able to demonstrate a difference in the strength of composite resin and porcelain crowns. Both the simulated fatigue experiment²⁰ and the numeric model are in agreement with these findings (risk of fracture below the value of 1 for both materials at 200 N). The prognosis of a restored tooth in the event of failure is another relevant consideration. The numeric model indicated that composite resin yielded lower risks of root fracture, as confirmed by the fatigue experiment. One possible explanation may be the ability of the composite resin to “buckle” under the load and absorb the stress by deformation, inducing the “lifting” of the buccal margin (as indicated by the tensile stress). However, the porcelain, with its more brittle behavior (less deformation), seems to have transferred the stress to the deeper portion of the root.

Small differences may remain between clinical reality and the virtual environment because of limitations such as the use of isotropic material properties for enamel and dentin, the boundary conditions around the root (absence of periodontal ligament), and the loading conditions. The loading condition in the present study was chosen to reproduce that of a previous experiment, and it should be emphasized that the conclusions are based on only this one loading condition. In spite of these limitations, numerical modeling is able to demonstrate the otherwise inaccessible stress distribution within the tooth-restoration

complex. It has been shown to be a useful tool for understanding tooth biomechanics and the biomimetic approach in restorative dentistry. The method is efficient and now within reach of clinicians. Because of the user-friendly graphic interfaces, it can be used for other medical applications to create models from another body part using either MRI, micro-CT, or cone beam CT data. This allows the generation of instant patient-specific models with predictive values for different restorative options. Furthermore, virtual prototyping can facilitate optimization and understanding of biomedical devices prior to animal and human clinical trials.

CONCLUSIONS

This investigation describes a virtual prototyping method for the generation of finite element models of dental structures and restorations. Interactive medical image processing and an advanced STL design and meshing software were used to generate a detailed 3-D model of a restored endodontically treated molar. Nonlinear contact analysis allowed simulation of a potential use of the model and confirmed its validity when compared to experimental data from simulated occlusal loading. The decreased risk of fracture and more favorable stress distribution of adhesive composite resin onlays compared to porcelain onlays is confirmed.

REFERENCES

1. Satava RM. The scientific method is dead—long live the (new) scientific method. *Surg Innov* 2005;12:173-6.
2. Ausiello P, Apicella A, Davidson CL, Rengo S. 3D-finite element analyses of cusp movements in a human upper premolar, restored with adhesive resin-based composites. *J Biomech* 2001;34:1269-77.
3. Ausiello P, Apicella A, Davidson CL. Effect of adhesive layer properties on stress distribution in composite restorations—a 3D finite element analysis. *Dent Mater* 2002;18:295-303.
4. Ausiello P, Rengo S, Davidson CL, Watts DC. Stress distributions in adhesively cemented ceramic and resin-composite Class II inlay restorations: a 3D-FEA study. *Dent Mater* 2004;20:862-72.
5. Cattaneo PM, Dalstra M, Frich LH. A three-dimensional finite element model from computed tomography data: a semi-automated method. *Proc Inst Mech Eng H* 2001;215:203-13.
6. Cattaneo PM, Dalstra M, Melsen B. The transfer of occlusal forces through the maxillary molars: a finite element study. *Am J Orthod Dentofacial Orthop* 2003;123:367-73.
7. Cattaneo PM, Dalstra M, Melsen B. The finite element method: a tool to study orthodontic tooth movement. *J Dent Res* 2005;84:428-33.
8. Tantbirojn D, Versluis A, Pintado MR, DeLong R, Douglas WH. Tooth deformation patterns in molars after composite restoration. *Dent Mater* 2004;20:535-42.
9. Versluis A, Tantbirojn D, Pintado MR, DeLong R, Douglas WH. Residual shrinkage stress distributions in molars after composite restoration. *Dent Mater* 2004;20:554-64.
10. Koriath TW, Versluis A. Modeling the mechanical behavior of the jaws and their related structures by finite element (FE) analysis. *Crit Rev Oral Biol Med* 1997;8:90-104.
11. Yaman SD, Alaçam T, Yaman Y. Analysis of stress distribution in a vertically condensed maxillary central incisor root canal. *J Endod* 1995;21:321-5.
12. Ko CC, Chu CS, Chung KH, Lee MC. Effects of posts on dentin stress distribution in pulpless teeth. *J Prosthet Dent* 1992;68:421-7.
13. Anusavice KJ, Hojjatie B, Dehoff PH. Influence of metal thickness on stress distribution in metal-ceramic crowns. *J Dent Res* 1986;65:1173-8.
14. Magne P, Versluis A, Douglas WH. Rationalization of incisor shape: experimental-numerical analysis. *J Prosthet Dent* 1999;81:345-55.
15. Verdonchot N, Fennis WM, Kuijs RH, Stolk J, Kreulen CM, Creugers NH. Generation of 3-D finite element models of restored human teeth using micro-CT techniques. *Int J Prosthodont* 2001;14:310-5.
16. Magne P. Efficient 3D finite element analysis of dental restorative procedures using micro-CT data. *Dent Mater* 2007;23:539-48.
17. Magne P, Tan DT. Incisor compliance following operative procedures: a rapid 3-D finite element analysis using micro-CT data. *J Adhes Dent* 2008;10:49-56.
18. Magne P, Oganesyan T. Premolar cuspal flexure as a function of restorative material and occlusal contact location. *Quintessence Int* 2009;40:363-70.
19. Magne P, Oganesyan T. CT scan-based finite element analysis of premolar cuspal deflection following operative procedures. *Int J Periodontics Restorative Dent* 2009;29:361-9.
20. Magne P, Knezevic A. Simulated fatigue resistance of composite resin versus porcelain CAD/CAM overlay restorations on endodontically treated molars. *Quintessence Int* 2009;40:125-33.
21. Magne P, Knezevic A. Influence of overlay restorative materials and load cusps on the fatigue resistance of endodontically treated molars. *Quintessence Int* 2009;40:729-37.

22. Akinmade AO, Nicholson JW. Poisson's ratio of glass-polyalkenoate ("glass-ionomer") cements determined by an ultrasonic pulse method. *J Mater Sci* 1995;6:483-5.
23. Anusavice KJ, Hojjatie B. Influence of incisal length of ceramic and loading orientation on stress distribution in ceramic crowns. *J Dent Res* 1988;67:1371-5.
24. Craig RG, Peyton FA, Johnson DW. Compressive properties of enamel, dental cements, and gold. *J Dent Res* 1961;40:936-45.
25. Eldiwany M, Powers JM, George LA. Mechanical properties of direct and post-cured composites. *Am J Dent* 1993;6:222-4.
26. Farah JW, Craig RG, Meroueh KA. Finite element analysis of three- and four-unit bridges. *J Oral Rehabil* 1989;16:603-11.
27. Friedman CE, Sandrik JL, Heuer MA, Rapp GW. Composition and physical properties of gutta-percha endodontic filling materials. *J Endod* 1977;3:304-8.
28. McGuinness NJ, Wilson AN, Jones ML, Middleton J. A stress analysis of the periodontal ligament under various orthodontic loadings. *Eur J Orthod* 1991;13:231-42.
29. Moroi, HH, Okimoto K, Moroi R, Terada Y. Numeric approach to the biomechanical analysis of thermal effects in coated implants. *Int J Prosthodont* 1993;6:564-72.
30. Nakayama WT, Hall DR, Grenoble DE, Katz JL. Elastic properties of dental resin restorative materials. *J Dent Res* 1974;53:1121-6.
31. Tam LE, Pulver E, McComb D, Smith DC. Physical properties of calcium hydroxide and glass-ionomer base and lining materials. *Dent Mater* 1989;5:145-9.
32. Yaman SD, Alaçam T, Yaman Y. Analysis of stress distribution in a vertically condensed maxillary central incisor root canal. *J Endod*. 1995;21:321-5.
33. Waltimo A, Könönen M. A novel bite force recorder and maximal isometric bite force values for healthy young adults. *Scand J Dent Res* 1993;101:171-5.
34. Waltimo A, Könönen M. Maximal bite force and its association with signs and symptoms of craniomandibular disorders in young Finnish non-patients. *Acta Odontol Scand* 1995;53:254-8.
35. Brunton PA, Cattell P, Burke FJ, Wilson NH. Fracture resistance of teeth restored with onlays of three contemporary tooth-colored resin-bonded restorative materials. *J Prosthet Dent* 1999;82:167-71.
36. Attia A, Abdelaziz KM, Freitag S, Kern M. Fracture load of composite resin and feldspathic all-ceramic CAD/CAM crowns. *J Prosthet Dent* 2006;95:117-23.

Corresponding author:

Dr Pascal Magne
University of Southern California
Division of Restorative Sciences
Herman Ostrow School of Dentistry, Oral Health Center
3151 S Hoover St
Los Angeles, CA 90089-7792
Fax: 213-821-5324
E-mail: magne@usc.edu

Acknowledgements

The author thanks Dan Wolf and Sunil Tahilramani (MSC Software Corp), and Erik Boelen and Jan Welkenhuyzen (Materialise) for their helpful suggestions.

Copyright © 2010 by the Editorial Council for
The Journal of Prosthetic Dentistry.

NOTEWORTHY ABSTRACTS OF THE CURRENT LITERATURE

Off-axis sliding contact reliability and failure modes of veneered alumina and zirconia

Santana T, Zhang Y, Guess P, Thompson VP, Rekow ED, Silva NR.
Dent Mater 2009;25:892-8.

Objective. All-ceramic dental crowns are popular because of their esthetics and biocompatibility. However, they often chip or fracture when subjected to repeated occlusal loading. Considerable efforts to improve the materials are being done through the study of fatigue and failure modes. The vast majority of fatigue studies have been conducted with uniaxial loading and no sliding action. We hypothesized different failure modes for porcelain veneered Y-TZP and that the reliability of porcelain veneered Y-TZP is higher than that of porcelain veneered alumina when subjected to fatigue under 30° off-axis sliding Y-TZP and alumina plates were porcelain veneered and cemented to aged composite blocks as a model for an all-ceramic crown on dentin.

Methods. Specimens ($n = 21$ per group) were fatigued at 30° off-axis with a hard sphere sliding contact in water, by means of a mouth-motion simulator apparatus.

Results. Although no difference between groups was found, the failure modes differed and there was a tendency to higher reliability for Y-TZP compared to alumina for a mission of 50,000 cycles at 150 N load.

Significance. Failure modes for alumina specimens were deep penetrating partial cone cracks and cementation internal surface radial cracks. Y-TZP specimens showed only surface damage with deep penetrating partial cone cracks extending to the veneer core interface, with no cementation surface radial cracking, which overall agrees with clinical finding. Angled sliding contact appears to better simulate oral function.

Reprinted with permission of the Academy of Dental Materials.